

# POISSON CLUSTER PROCESS MODELS FOR DETECTING ULTRA-DIFFUSE GALAXIES

BY DAYI LI<sup>1,a</sup> , ALEX STRINGER<sup>2,b</sup> , PATRICK E. BROWN<sup>1,3,c</sup> , GWENDOLYN M.  
EADIE<sup>1,4,d</sup>  AND ROBERTO G. ABRAHAM<sup>4,5,e</sup> 

<sup>1</sup>Department of Statistical Sciences, University of Toronto, <sup>a</sup>[dayi.li@mail.utoronto.ca](mailto:dayi.li@mail.utoronto.ca)

<sup>2</sup>Department of Statistics and Actuarial Sciences, University of Waterloo, <sup>b</sup>[alex.stringer@uwaterloo.ca](mailto:alex.stringer@uwaterloo.ca)

<sup>3</sup>Center for Global Health Research, St. Michael's Hospital, <sup>c</sup>[patrick.brown@utoronto.ca](mailto:patrick.brown@utoronto.ca)

<sup>4</sup>David A. Dunlap Department of Astronomy & Astrophysics, University of Toronto, <sup>d</sup>[gwen.eadie@utoronto.ca](mailto:gwen.eadie@utoronto.ca)

<sup>5</sup>Dunlap Institute for Astronomy & Astrophysics, University of Toronto, <sup>e</sup>[roberto.abraham@utoronto.ca](mailto:roberto.abraham@utoronto.ca)

We propose a novel set of Poisson Cluster Process models to detect Ultra-Diffuse Galaxies, a recently-discovered class of galaxies that are challenging to detect and are of substantial interests in modern astrophysics. We construct an improved spatial birth-death-move MCMC algorithm to make inferences about the locations of these otherwise un-observable galaxies. Our novel models significantly out-perform existing approaches based on the Log-Gaussian Cox Process; the novel marked point process we propose can also improve the detection performance for UDGs in noisy environments. We find evidence of a potential new “dark galaxy” that was not detected using previous methods.

**1. Introduction.** Ultra-diffuse galaxies (UDGs) are a class of galaxies first defined in 2015 (Van Dokkum et al., 2015) with extremely low-surface brightness. Although a small sample of similar galaxies were known for decades (e.g., Binggeli et al., 1984), attention and interest towards UDGs have been rising significantly recently since a large number of them were detected using the specially designed Dragonfly Telephoto Array (Abraham and van Dokkum, 2014). Since they lack baryonic matter <sup>1</sup> (Van Dokkum et al., 2015; Yagi et al., 2016; Martínez-Delgado et al., 2016; Venhola et al., 2017; Wittmann et al., 2017; Janssens et al., 2019; Lim et al., 2020) compared to other types of normal, brighter galaxies, UDGs have gained substantial scientific interests as they are the perfect venues for studying dark matter (Hui et al., 2017; van Dokkum et al., 2019; Wasserman et al., 2019; Burkert, 2020), one of the biggest mystery in modern astronomy and cosmology.

UDGs typically appear as faint light patches in astronomical images. Figure 1 shows some example UDGs and their comparison in terms of physical sizes and surface brightness to some typical bright, normal galaxies. The low surface brightness nature of UDGs as shown in Figure 1 means detecting them is difficult, and a major endeavor in astronomy currently is to devise efficient and accurate method to detect as many UDGs as possible.

Presently, UDGs are detected by an exhaustive search of their diffuse stellar light. However, such a method requires long telescope observing time on the orders of hours or days to obtain high quality images, and is thus inefficient and costly. Systematic imaging artefacts and light-reflecting gas clouds can also cause false positive detections which require extensive human labour to discern. Moreover, UDGs in the nearby Universe ( $d \leq 10$  Mpc <sup>2</sup>), if

---

*Keywords and phrases:* Point Processes, Ultra-Diffuse Galaxies, Astrostatistics.

<sup>1</sup>Baryonic matter is matter that interacts with electromagnetic radiation, e.g., stars, planets, gas, and dust, etc.

<sup>2</sup>Mpc is a standard distance unit that stands for Mega-Parsec. 1 Mpc equates to  $\sim 3.26$  million light-years.

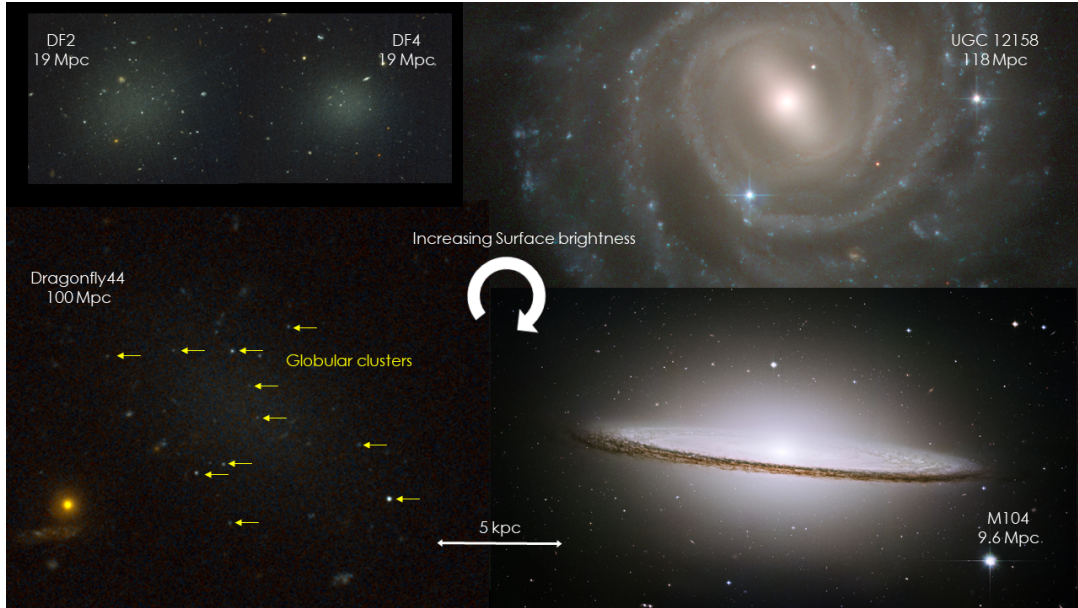


Fig 1: Three UDGs (Dragonfly 44, NGC 1052-DF2, NGC 1052-DF4) and two other typical bright, normal galaxies (UGC 12158, M104). The galaxies are arranged in clockwise order of increasing surface brightness, and adjusted to be on the same physical scales. Numbers below the galaxy IDs are the distances of the galaxies. UGC 12158 is shown since it is considered to resemble our own Milky Way galaxy in appearance. M104 is a bright galaxy that has a light profile resembling an UDG the most, except for its brightness and the galactic disk. Arrows in the image of Dragonfly 44 indicate some of its globular clusters.

they exist, cannot be detected in such a way since the diffuse stellar light of UDGs shown in Figure 1 will become resolved individual stars.

Most importantly, the current method of detecting UDGs assumes they have associated diffuse stellar light. However, this assumption has no physical basis since “dark” galaxies with (almost) no individual field stars have long been expected to exist (e.g., Oosterloo, T. A., Heald, G. H. and de Blok, W. J. G., 2013; Cannon et al., 2015; Janowiecki et al., 2015). If such galaxies exist, their discovery will be groundbreaking, but they will never be found using the current method of looking for diffuse stellar light. Therefore, novel method is in need for detecting galaxies that does not depend on the unsubstantiated assumption that they must have diffuse stellar light.

Recently, Li et al. (2022) detected UDGs through the spatial clustering signals of their associated globular clusters (GCs) using log-Gaussian Cox process (LGCP; Møller, Syversveen and Waagepetersen, 1998). GCs are compact, spheroidal agglomeration of hundreds of thousands of stars bound together by gravity. GCs are easy to detect from existing massive all-sky surveys. Many UDGs were found to contain an abundance of GCs (van Dokkum et al., 2016; Peng and Lim, 2016; Amorisco et al., 2018; Lim et al., 2018, 2020; Danieli et al., 2021) where they appear as bright point sources as indicated in Dragonfly 44 shown in Figure 1.

Based on this observation, Li et al. introduced a point process model for detecting UDGs. Let  $\mathbf{X} = \{x_1, \dots, x_n\}$  denotes the random locations of GCs within an observational window  $S \subset \mathbb{R}^2$ , taken here to be an astronomical image. Let  $\lambda(s) > 0, s \in S$  be the intensity function of  $\mathbf{X}$ , which is the mean number of points per unit area at  $s$ . Li et al. constructed the following LGCP for  $\mathbf{X}$ :

$$\mathbf{X} \sim \text{IPP}(\lambda(s)),$$

$$\begin{aligned}\log \lambda(s) &= \beta_0 + f_{\text{gal}}(s; \boldsymbol{\beta}) + \mathcal{U}(s), \\ \mathcal{U}(s) &\sim \mathcal{GP}(0, \sigma^2 \mathbf{C}(\cdot; h)), \\ \mathbf{C}(|s - t|; h) &= \mathcal{M}(|s - t|/h), \quad s, t \in \mathbb{R}^2.\end{aligned}$$

IPP denotes inhomogeneous Poisson process.  $\beta_0$  is the intercept for the log-intensity,  $f_{\text{gal}}$  is a covariate term that accounts for the clustering signals of GCs from known, bright galaxies (see [Li et al. \(2022\)](#) for details). The presence of UDGs are then considered as unexplained clustering signals captured within  $\mathcal{U}(s)$  which is a zero-mean spatial Gaussian process with a Matérn covariance function. The detection of UDGs is done by looking for regions with high values of  $\mathcal{U}(s)$  using the excursion function introduced by [Bolin and Lindgren \(2015, 2018\)](#).

Although [Li et al.](#) showed that LGCP can detect UDGs, it suffers from several limitations:

1. LGCP is an inherently clustered point process, and there is no principled way to tell when there is no UDGs in the data. [Li et al.](#) determined this by eyes based on the posterior distribution of  $\mathcal{U}(s)$ , which is undesirable.
2.  $\mathcal{U}(s)$  within LGCP arises from a Gaussian process, and it may miss out on the weaker GC clustering signals as the model may consider weak signals as inevitable fluctuations from the underlying Gaussian process.
3. Detection performance degrades when the environment becomes noisy — there are more non-UDG GCs — as confirmed by simulation studies done by [Li et al.](#).

We propose two novel point process models to detect UDGs based on the Poisson cluster process (PCP) framework. The first model is intended to solve the issues of 1 and 2. It addresses issue 1 as PCP can determine on its own whether the data contains clusters or not. It overcomes issue 2 as there is no inherent fluctuations of intensity in PCP. The intuitive physical modelling strategy based on astronomical observations ensures detections of weaker clustering signals.

The second model is a marked point process model extended from the first one where we employ the GC colour information as marks in the hope of improving UDG detection in noisy environments. The colour of a GC is a surrogate measure of its chemical composition. It is understood that GCs within UDGs were generally formed in the same environments and time periods (e.g. [Lotz, Miller and Ferguson, 2004](#)). Therefore, GCs within UDGs should not only exhibit spatial clustering, they should also have low colour variation compared to GCs from other environments. By adding information of GC colour variation, one may be able to improve UDG detection. We need to note that the claim of GCs within UDGs having low colour variations is not universal as such an observation is an average tendency. Thus, there are UDGs not conforming with such an observation, although these are the minority.

To conduct inference about the locations of UDGs using our proposed models, we design an improved spatial birth-death-move Markov chain Monte-Carlo (MCMC) algorithm based on the algorithm proposed by [Møller and Torrisi \(2005\)](#). The algorithm by [Møller and Torrisi](#) is a variant of the reversible jump MCMC ([Green, 1995](#)) for fitting shot noise Cox process ([Møller, 2003](#); [Møller and Torrisi, 2005](#)). Our proposed models, however, are much more complicated which renders the algorithm by [Møller and Torrisi](#) sub-optimal. Thus, we combine an adaptive MCMC proposal ([Roberts and Rosenthal, 2009](#)) with a set of empirically tuned proposal densities to improve the convergence of Markov chains.

We fit our models using our proposed MCMC algorithm to a set of real GC data obtained from a *Hubble Space Telescope (HST)* imaging survey to demonstrate that our models are indeed superior than LGCP and the inclusion of GC colour information has the potential to significantly improve the detection performance.

**2. Data Description.** The purpose of this paper is to introduce our proposed models for UDGs detection, and thus we consider data that contain previously known UDGs to test our models. The data used in this paper come from the Program for Imaging of the PERseus cluster (PIPER; [Harris et al. 2020](#)), which are the same data used in [Li et al. \(2022\)](#). The survey was conducted using the *HST* Advanced Camera for Surveys (ACS) and Wide Field Camera 3 (WFC3). The target region is the Perseus galaxy cluster at a distance of 75 Mpc ([Gudehus, 1995](#); [Hudson et al., 1997](#)). The data consist of 10 imaging visits. Each visit contains two imaging pointings taken by ACS and WFC3 respectively. The images are taken using F475W, F475X, and F814W filters that capture different wavelengths of light. Each imaging pointing has an associated ID, for example, V6-ACS stands for the image taken by the ACS on the 6-th visit. The detailed extraction procedures of GCs from the images are described in [Li et al. \(2022\)](#) as well as [Harris et al. \(2020\)](#). Each image is roughly a square with approximately 4300 pixels per side. For simplicity, we scale all the imaging fields and the corresponding GC point patterns to a  $[0, 1]^2$  square.

The colour of a GC is defined as the difference between its magnitude in different wavelengths of light. Here it is the difference between the magnitude in F475W and F814W:

$$C = \text{F475W} - \text{F814W}.$$

For images taken with WFC3, only magnitude measurement in F475X is available instead of F475W. A transformation ([Harris et al., 2020](#)) is applied to F475X to obtain the equivalent magnitude in F475W. We need to note that the GC colour  $C$  is not the data we directly use in our model. Instead, what is used is the GC colour variation  $V$  which is derived from  $C$ . The details of obtaining the GC colour variation is contained in the supplementary materials.

To validate UDGs detected by our method, we use the UDG catalog from [Wittmann et al. \(2017\)](#), as well as an unpublished UDG catalog obtained by A. Romanowsky. Hereafter, we refer to the UDGs from [Wittmann et al. \(2017\)](#) as WUDGs and UDGs from Romanowsky as RUDGs. The identifiers of objects from these catalogs are WUDG-# and RUDG-#, where "#" is the ID number from the catalogs.

**3. Our Method using Poisson Cluster Process.** Here we describe the basic structure of a PCP and present our proposed models.

3.1. *Basic PCP.* A PCP is a type of hierarchical process with three levels of hierarchy: for the first level of the hierarchy, the cluster centers come from a parent point process which is assumed to be a Poisson process; the second level of the hierarchy generates a random count associated with each parent point. Conditional on the random count  $N$  and the parent point location  $c$ ,  $N$  number of offspring points are IID generated according to some probability density function centered at the parent point  $c$  and the offspring points are observed.

Let  $\mathbf{X}$  denote the offspring point process and  $\mathbf{X}_c$  be the parent point process.  $\lambda(s) > 0$ ,  $s \in \mathbb{R}^2$  is the corresponding intensity function of  $\mathbf{X}$ , and  $\lambda_c > 0$  the intensity of  $\mathbf{X}_c$ . A PCP can be written as:

$$\begin{aligned} \mathbf{X} \mid \lambda &\sim \text{IPP}(\lambda(s)), \\ \lambda(s) \mid \mathbf{X}_c &= \sum_{j=1}^J N_j h_j(s - c_j), \\ \mathbf{X}_c &\sim \text{HPP}(\lambda_c). \end{aligned}$$

$N_j$  is the average number of points from cluster  $j$  and  $h_j$  is a probability density function on  $\mathbb{R}^2$  centered at the origin. We have  $\mathbf{X}_c = \{c_1, \dots, c_J\}$  where  $J$  is the total number of clusters which is random, and  $\mathbf{X}_c$  is assumed to be a homogeneous Poisson process (HPP).

3.2. *Models.* Denote  $\Xi = (\beta_0, \Gamma, \Upsilon)$ ,  $\Gamma = \{\mathbf{G}_k\}_{k=1}^{N_G}$ ,  $\Upsilon = \{\mathbf{U}_j\}_{j=1}^{N_c}$ , and  $\Sigma = \{\sigma_j\}_{j=0}^{N_c}$  where  $\mathbf{G}_k = (N_k^g, R_k^g, n_k^g, e_k^g, \varphi_k^g)$ ,  $\mathbf{U}_j = (N_j^u, R_j^u, n_j^u, e_j^u, \varphi_j^u)$ , whose meanings will be explained later, we propose the following two models for detection of UDGs:

**Model 1 (Unmarked Process):**

$$\begin{aligned} \mathbf{X} \mid \lambda &\sim \text{IPP}(\lambda(s)), \\ \lambda(s) \mid \mathbf{X}_c, \Xi &= \beta_0 + \sum_{k=1}^{N_G} f(s; c_k, \mathbf{G}_k) + \sum_{j=1}^{N_c} f(s; x_{c,j}, \mathbf{U}_j), \\ \mathbf{X}_c &\sim \text{HPP}(\lambda_c), \end{aligned}$$

**Model 2 (Marked Process):**

$$\begin{aligned} \mathbf{X} \mid \lambda &\sim \text{IPP}(\lambda(s)), \\ \lambda(s) \mid \mathbf{X}_c, \Xi &= \beta_0 + \sum_{k=1}^{N_G} f(s; c_k, \mathbf{G}_k) + \sum_{j=1}^{N_c} f(s; x_{c,j}, \mathbf{U}_j), \\ V(\mathbf{x}_i) \mid \mathbf{x}_i, \mathbf{X}_c, \Xi, \Sigma &\sim \sum_{j=0}^{N_c} p_{ij}^1 \mathcal{N}(0, \sigma_j^2), \\ p_{ij}^1 &= \mathbb{P}(Z_i = j \mid \mathbf{x}_i, \mathbf{X}_c, \Xi, \Sigma), \\ \mathbf{X}_c &\sim \text{HPP}(\lambda_c). \end{aligned}$$

For the above two models, Model 1 is the model for detecting UDGs purely through GC point patterns. Model 2 is the marked point process model designed to incorporate GC colour information aimed to improve the detection of UDGs in noisy environments. We explain below the parameters and structural details of Model 1 and 2.

3.2.1. *Modelling Intensity Function  $\lambda(s)$ .* In Model 1 and Model 2, the intensity function of the GCs is assumed to be the sum of intensity functions of GCs from the following three different environments: (a) ultra-diffuse/"dark" galaxies, (b) bright, normal galaxies, and (c) intergalactic medium. We assume the observed point pattern of GCs come from independent superposition of GC point patterns from each of the above environments.

- **Ultra-Diffuse/"Dark" Galaxies:** The most common model used for modelling the intensity of GCs within UDGs is the Sérsic profile (Sérsic, 1963; Peng and Lim, 2016; van Dokkum et al., 2018; Danieli et al., 2021). Sérsic profile describes how the intensity of GCs within galaxies falls off as one moves away from the center of the galaxy. The Sérsic profile has six parameters:

1.  $c$ : the center of the galaxy,
2.  $N$ : the average number of GCs from the galaxy,
3.  $R$ : characteristic size of the GC system,
4.  $n$ : the Sérsic index which describes how concentrated the GCs distribute around the center of the galaxy,
5.  $e$ : aspect ratio of the GC system (ratio of the major axis to the minor axis),
6.  $\varphi$ : the orientation angle of the galaxy.

Given all of the above parameters, the Sérsic profile is given by

$$f(s; c, (N, R, n, e, \varphi)) = \frac{N}{2\pi R^2 n \Gamma(2n) e} \exp\left(-\left(\frac{r(s)}{R}\right)^{1/n}\right),$$

where  $r^2(s) = ((s_{(1)} - c_{(1)}) \cos(\varphi) - (s_{(2)} - c_{(2)}) \sin(\varphi))^2 + ((s_{(1)} - c_{(1)}) \sin(\varphi) + (s_{(2)} - c_{(2)}) \cos(\varphi))^2 / e^2$  and  $s = (s_{(1)}, s_{(2)})$ ,  $c = (c_{(1)}, c_{(2)}) \in \mathbb{R}^2$ . The subscripts and superscripts of the six parameters for the Sérsic profile presented in Model 1 and Model 2 are omitted here for simplicity.  $f$  is the intensity function under the Sérsic profile, which gives the intensity of GCs at any location  $s \in \mathbb{R}^2$ .  $s_{(1)}$  and  $s_{(2)}$  are the horizontal and vertical coordinate of  $s$  respectively.  $r(s)$  describes an ellipse centered at  $c$  with orientation  $\varphi$  and aspect ratio  $e$ . In our models, all of the above physical parameters for UDGs are treated as unknown since UDGs are the main objects we aim to detect, thus we should not assume any information about them is known.

Under Model 1 and Model 2,  $\sum_{j=1}^{N_c} f(s; x_{c,j}, \mathbf{U}_j)$  is the term that models the intensity of GCs from UDGs where  $N_c$  denotes the random number of UDGs.

- **Bright, normal Galaxies:** The main types of bright galaxies we encounter in the context of our problem are elliptical galaxies. As the name suggests, this type of galaxies have ellipsoidal shape, and the distribution of GCs from these galaxies typically follow a similar structure (Harris, 1991; Wang et al., 2013). GCs are most abundant in elliptical galaxies, we thus need to account for their effect in the intensity function. Otherwise, their signals will dominate the signals of UDGs.

We adopt the same Sérsic profile for the intensity of GCs from elliptical galaxies. However, we treat  $c$ ,  $e$ , and  $\varphi$  for elliptical galaxies as known. These parameters can be measured with very high accuracy based on the light distribution of elliptical galaxies using standard source extraction software such as SExtractor (Bertin and Arnouts, 1996). GC system of an elliptical galaxy generally shares these three parameters with the light distribution of the galaxy (Harris, 1991; Wang et al., 2013). Hence, it is reasonable to treat these three parameters as known. For the rest of the parameters, accurate estimates are unavailable, and they are considered unknown parameters in the model.

In our models,  $\sum_{k=1}^{N_G} f(s; c_k, \mathbf{G}_k)$  models the intensity function of GCs from normal galaxies.  $N_G$  is the number of normal galaxies in an observation field.

- **Intergalactic Medium:** For GCs from the intergalactic medium, we model them as a HPP with constant intensity  $\beta_0 > 0$ .

**3.2.2. Incorporating GC Colours.** In Model 2,  $\mathbf{x}_i$  is the location of the  $i$ -th GC while  $V(\mathbf{x}_i)$  the colour variation of the  $i$ -th GC. We model the conditional distribution of  $V$  given all other information using a mixture model where each mixture component is a zero-mean Gaussian random variable. The mixture components represent which environment the  $i$ -th GC comes from, specified by an indicator variable  $Z_i$  where  $Z_i = 0$  represents the  $i$ -th GC belonging to the background or a normal galaxy, while  $Z_i > 0$  represents the GC coming from one of the  $N_c$  UDGs. By the law of total probability,

$$\pi(V(\mathbf{x}_i) | \mathbf{x}_i, \mathbf{X}_c, \mathbf{\Xi}, \mathbf{\Sigma}) = \sum_{j=0}^{N_c} p_{ij}^1 \pi(V(\mathbf{x}_i) | Z_i = j, \mathbf{x}_i, \mathbf{X}_c, \mathbf{\Xi}, \mathbf{\Sigma}).$$

Given  $Z_i = j$ , we have  $V(\mathbf{x}_i) \sim \mathcal{N}(0, \sigma_j^2)$ .  $p_{ij}^1$  is the full conditional probability that the  $i$ -th GC comes from the  $j$ -th environment under Model 1, which we call the GC membership probability of Model 1.  $p_{ij}^1$  has the following expression

$$p_{ij}^1 = \mathbb{P}(Z_i = j | \mathbf{x}_i = x_i, \mathbf{X}_c, \mathbf{\Xi}, \mathbf{\Sigma}) = \frac{\lambda_j(x_i)}{\sum_{k=0}^{N_c} \lambda_k(x_i)} = \frac{\lambda_j(x_i)}{\lambda(x_i)},$$

where  $\lambda_j$  denotes the intensity of the  $j$ -th environment. Derivation of  $p_{ij}^1$  is in the supplementary materials. If we also condition on the colour variations of GCs, we obtain the mem-

bership probability of Model 2  $p_{ij}^2$ :

$$p_{ij}^2 = \mathbb{P}(Z_i = j \mid \mathbf{x}_i = x_i, V(\mathbf{x}_i), \mathbf{X}_c, \Xi, \Sigma) = \frac{\sigma_j^{-1} \exp\left(-V(x_i)^2/2\sigma_j^2\right) \lambda_j(x_i)}{\sum_{k=0}^{N_c} \sigma_k^{-1} \exp\left(-V(x_i)^2/2\sigma_k^2\right) \lambda_k(x_i)}.$$

Derivation of the above is also in the supplementary materials.  $p_{ij}^1$  and  $p_{ij}^2$  are presented explicitly here since they are not parameters that can be specified with freedom by users but rather fully determined by other parameters in our models. Furthermore, due to the nature of our MCMC inference algorithm which will be discussed later,  $p_{ij}^1$  and  $p_{ij}^2$  are useful for conducting MCMC convergence diagnostics of our models.

The biggest advantage of our model is that it provides us with the ability to explicitly enforce the assumption that GC colour variation within UDGs is smaller than that of GCs in other environments. Since the variance term  $\sigma_j^2$  characterizes how large the colour variation is for GCs in each environment, we can directly impose condition on the prior distributions of  $\{\sigma_j\}_{j=0}^{N_c}$  with  $\sigma_0 > \sigma_j, \forall j > 0$  so that the assumption of GC colour variation in UDGs being smaller is easily enforced.

Moreover, by using a PCP, it grants us the ability to construct direct physical model of the intensity functions of UDGs and explicit GC membership assignments. It is then possible for us to introduce the mixture model for the GC colour variations. This contributes to another advantage of our models over the LGCP framework, since it is impossible to provide direct physical model for the intensity functions of UDGs under LGCP as it is driven entirely by a Gaussian process. Thus, the GC membership assignment does not exist for LGCP and the inclusion of GC colour information is not possible.

**3.3. Priors.** Many physical parameters (such as  $N, R$ ) in our models are well-studied in astronomical literature, and they are characterised by log-normal (LN) distributions (see [Shen et al., 2003](#); [Harris, Harris and Alessi, 2013](#), for example).

For  $\lambda_c$ , which describes how many UDGs there are in a pointing, we set  $\lambda_c \sim \text{LN}(\log(l_c), 0.2^2)$ . The specific value of  $l_c$  is uncertain ([Lim et al., 2018](#); [Venhola et al., 2017](#); [Lim et al., 2020](#)), but it should be low ( $l_c \leq 3$ ). We choose a different value of  $l_c \in \{1, 2, 3\}$  for different pointing: pointings with more GCs have higher values of  $l_c$  since they are more likely to contain UDGs. The details for setting  $l_c$  is given in supplementary materials.

For  $N_j^u$ , we set  $N_j^u \sim \text{LN}(\log(N^u), 1)$  with  $3 \leq N^u \leq 10$  for different imaging pointings due to the wide range of UDG GC counts (see [van Dokkum et al., 2016](#); [Amorisco et al., 2018](#); [Lim et al., 2018, 2020](#), for example) and uncertainty ([Lim et al., 2018, 2020](#); [Danieli et al., 2021](#)). Prior analysis for  $N_j^u$  is given in supplementary materials. For  $R_j^u$ , we set  $R_j^u \sim \text{LN}(\log(0.02), 0.5^2)$  based on the typical size of an UDG ([Van Dokkum et al., 2015](#)). For the rest of the parameters, we set  $n_j^u \sim \text{LN}(\log(1), 0.75^2)$ ,  $e_j^u \sim \text{LN}(\log(1.1), 0.3^2)$  based on previous studies (e.g. [Burkert, 2017](#); [Prole et al., 2019](#)) while  $\varphi_j^u \sim \text{Uniform}(0, \pi)$ . For  $\sigma_j$ 's which describes the magnitude of the GC colour variations, we set

$$\begin{aligned} \sigma_0 &\sim \text{Gamma}(0.2, 0.05), \\ \sigma_j \mid \sigma_0 &\sim \text{Uniform}(0, \sigma_0), \quad j > 0, \end{aligned}$$

based on the previous extensive studies on GC colours (see [Gebhardt and Kissler-Patig, 1999](#), for example) and the assumption that  $\sigma_j$ 's are smaller than  $\sigma_0$ .

For the normal galaxies, we set  $N_k^g \sim \text{LN}(\log(\mathcal{N}_g^k), 0.25^2)$  where  $\mathcal{N}_g^k$  is determined based on the specific frequency relation ([Harris, 1991](#)). For  $R_k^g$ , we set  $R_k^g \sim \text{LN}(\log(\mathcal{R}_g^k), 0.25^2)$  where  $\mathcal{R}_g^k$  is obtained based on the results from [Forbes \(2017\)](#). For  $n_k^g$ , we set  $n_k^g \sim \text{LN}(\log(0.5), 0.5^2)$ .

Lastly, for the intensity parameter  $\beta_0$  of the intergalactic medium, we provide it with a prior of  $\beta_0 \sim \text{LN}(\log(b_0), 0.25^2)$ .  $b_0$  is different for different pointings as it is chosen to maintain the physical reality that the number of GCs in UDGs, normal galaxies, and the intergalactic medium equate to the total number of GCs in each point pattern.

**4. Inference & Estimation.** Since our problem is a prediction problem, we require a full posterior predictive distribution to undertake such a task. This requires us to conduct full Bayesian inference. Traditionally, PCP models are fitted using moment-matching or maximum likelihood based approaches (e.g. Waagepetersen, 2007; Møller and Toftaker, 2014; Diggle et al., 2013) for parameter estimation problems. But for full Bayesian inference and cluster center detection, the task is much more difficult. Rather a limited amount of works (e.g. Castelleo, 1998; Møller and Toftaker, 2014) similar to ours have previously managed to conduct full Bayesian inference on real-life data sets using the reversible jump MCMC (RJMCMC; Green 1995) or its variants. However, the models considered in previous works are much simpler than the ones we propose, thus the inference algorithm would not be optimal for our purpose. More recently, mixture of finite mixture models have been leveraged (Geng, Shi and Hu, 2021; Wang et al., 2022) so that a collapsed Gibbs sampling algorithm can be used for fast inference. But such a method imposes distributional assumption on the parameters in order for the Gibbs sampler to work, and is thus not flexible enough for models as complex as ours. Therefore, we design a RJMCMC-type algorithm that is more suited for our models while being sufficiently flexible.

#### 4.1. Inference through Spatial Birth-Death-Move MCMC.

4.1.1. *Spatial Birth-Death-Move MCMC by Møller and Torrisi.* To conduct inference for our model, we construct a specialized and improved spatial birth-death-move MCMC algorithm based on the one proposed by (Møller and Torrisi, 2005). The algorithm by Møller and Torrisi is sub-optimal for our problem due to the following reasons:

- Møller and Torrisi only considered models without any fixed-dimensional parameters such as  $\beta_0$  in our model. The inclusion of fixed-dimensional parameters in our models can hamper the mixing of the chain. Thus, we introduce an adaptive MCMC update scheme (Roberts and Rosenthal, 2009) for the fixed-dimensional parameters in our models.
- The proposal distributions for the trans-dimensional parameters by Møller and Torrisi are too simple and can lead to convergence issue. Thus, we modify these to improve Møller and Torrisi’s algorithm.

4.1.2. *An Improved Spatial Birth-Death-Move MCMC algorithm.* At each update step of the spatial birth-death-move MCMC, one can propose to add a new UDG (birth), remove an existing UDG (death), or tweak the configuration of one of the existing UDGs (move). We illustrate our constructed algorithm based on Model 2. The algorithm for Model 1 will be almost identical. Let  $\Theta$  denotes all the parameters that are fixed-dimensional: these are the parameters that are not associated with UDGs. Under Model 2, we have  $\Theta = (\beta_0, \lambda_c, \Gamma, \sigma_0)$ . Let  $\Phi$  denote the rest of the parameters where  $\Phi = \{(x_{c,1}, \mathbf{U}_1, \sigma_1), \dots, (x_{c,N_c}, \mathbf{U}_{N_c}, \sigma_{N_c})\}$ .  $\Phi$  has varying dimension as  $N_c$  is random. Assume now that  $N_c$  is temporarily fixed. Then the posterior distribution with fixed  $N_c$  is

$$\pi(\Theta, \Phi | \mathbf{X}, \mathbf{V}) \propto \exp\left(|S| - \int_S \lambda(s) ds\right) \prod_{i=1}^n \lambda(x_n) \times \prod_{i=1}^n \left[ \sum_{j=0}^{N_c} p_{ij}^1 \sigma_j^{-1} \exp(-V(x_i)^2 / 2\sigma_j^2) \right] \pi(\Theta, \Phi).$$

The associated prior distribution  $\pi(\Theta, \Phi)$  is given by

$$\pi(\Theta, \Phi) = \exp(|S|(1 - \lambda_c)) \left(\frac{\lambda_c}{\sigma_0}\right)^{N_c} \left[ \prod_{j=1}^{N_c} \pi(\sigma_j | \sigma_0) \pi(\mathbf{U}_j) \right] \left[ \prod_{k=1}^{N_G} \pi(\mathbf{G}_k) \right] \pi(\beta_0) \pi(\lambda_c) \pi(\sigma_0).$$

Derivation of the above is given in supplementary materials. The same quantity under Model 1 is similar but with all components related to GC colour variations dropped. The integration of the intensity  $\lambda(s)$  on  $S$  in the likelihood is carried out by

$$\int_S \lambda(s) ds \approx \sum_{\ell=1}^L |A_\ell| \lambda(c_\ell),$$

where  $\{A_\ell\}_{\ell=1}^L$  is a fine-grid discretising  $S$  with  $c_\ell$  being the center of  $A_\ell$ .

Assume the state of the chain is  $(\Theta, \Phi)$  at an update step. We set the probabilities for birth, death, and move proposal to be  $p_b = p_d = p_m = 1/2$ . If a birth proposal is chosen, we then uniformly generate a location  $x$  for the new UDG within  $S$ . We generate its associated Sérsic profile parameters  $\mathbf{U}$  and the colour variation parameter  $\sigma$  according to some proposal densities  $q_b^u(\cdot)$  and  $q_b^s(\cdot)$  respectively. In our implementation, these are set to their corresponding prior distributions. Furthermore, we propose a new state  $\Theta'$  for  $\Theta$  according to a proposal density  $q_\theta(\cdot | \cdot)$  based on an adaptive MCMC scheme which we illustrate below. The birth-death Metropolis-Hasting ratio is then:

$$r[(\Theta, \Phi), (\Theta', (x, \mathbf{U}, \sigma))] = \frac{\pi(\Theta', \Phi \cup \{(x, \mathbf{U}, \sigma)\} | \mathbf{X}, \mathbf{V}) q_\theta(\Theta | \Theta') |S|}{\pi(\Theta, \Phi | \mathbf{X}, \mathbf{V}) (|\Phi| + 1) q_\theta(\Theta' | \Theta) q_b^u(\mathbf{U}) q_b^s(\sigma)}.$$

Due to space constraint, the details of our MCMC algorithm is illustrated in Algorithm 1 in the supplementary materials.

The adaptive MCMC proposal for  $\Theta$  we employ is given below:

$$\Theta_{i+1} | \Theta_i \sim \begin{cases} \mathcal{N}(\Theta_i, C_\theta) & i \leq 1000, \\ \mathcal{N}(\Theta_i, \gamma \text{Cov}(\{\Theta_j\}_{j=1}^i)) & 1000 < i \leq 10000, \\ \mathcal{N}(\Theta_i, \gamma \text{Cov}(\{\Theta_j\}_{j=1}^{10000})) & i > 10000. \end{cases}$$

$C_\theta$  is a diagonal matrix and  $\gamma > 0$  is a scaling factor, both of which are user-defined. All components of  $\Theta$  are transformed into log-scale for the ease of proposal generation.

In the algorithm proposed by Møller and Torrisi (2005), the proposal densities of  $x$  in the move step is an uniform distribution over  $S$ . This is inefficient since the main purpose of employing a move step is to tweak the configuration of an existing cluster. If the move proposal of  $x$  is from a uniform distribution, it will get rejected with high probability if the center of the cluster chosen to be tweaked is already close to the center of an existing UDG. This makes the chain more likely to get stuck and mixing to be poor. Hence, we set the move step proposal densities to be conditional on the parameters of the UDG that is chosen to be tweaked. Thus, the birth step in our algorithm has the purpose of sufficiently exploring the parameter space associated with UDGs while the move step is used for the fine-tuning of these parameters.

## 4.2. Estimation.

4.2.1. *UDG Detection.* We first need to determine whether a pointing contains UDGs at certain locations. Let  $\mathbf{D} = \mathbf{X}$  or  $(\mathbf{X}, \mathbf{V})$  depending on whether Model 1 or Model 2 is considered. We compare (i)  $\mathbb{P}(N_c = 0 | \mathbf{D})$  and (ii) the posterior probability an UDG exists at a

certain location. Comparing  $\mathbb{P}(N_c = 0 \mid \mathbf{D})$  to  $\mathbb{P}(N_c = k \mid \mathbf{D})$  for some  $k > 0$  is not a suitable rule to determine the existence of UDGs due to the well-known label-switching problem (Jasra, Holmes and Stephens, 2005) of RJMCMC-type algorithms. For example, the posterior samples of  $N_c = 1$  can represent multiple spurious clusters of GCs at different locations, thus  $N_c = 1$  does not mean an actual UDG exists. We estimate (i) using the proportion of  $N_c = 0$  in the posterior sample of  $N_c$ . For (ii), we estimate

$$\mathbb{P}(\text{UDG in } \omega \mid \mathbf{D}) = \mathbb{P}(\text{UDG in } \omega \mid \mathbf{D}, N_c > 0)(1 - \mathbb{P}(N_c = 0 \mid \mathbf{D})),$$

for any fixed region  $\omega \subset S$  where  $\omega$  has a size that can only contain no more than one UDG. We first discretise  $S$  into equal-sized cells  $\omega_i$ . We then estimate the first term in the RHS above by the ratio of the number of sampled UDG centers in  $\omega_i$  to the total number of sampled UDG centers. If the maximum of the estimated quantity for all  $\omega_i$  is smaller than the estimate of  $\mathbb{P}(N_c = 0 \mid \mathbf{D})$ , we conclude there is no UDG in the pointing and vice versa. For the cell size, we set it to have 10 kpc width based on the size distribution of known UDGs. This size makes sure that all the sampled UDG centers in a cell represent the same UDG, but not too small that the estimated probability is arbitrarily smaller than  $\mathbb{P}(N_c = 0 \mid \mathbf{D})$ .

If we determine that a pointing contains UDGs, we construct the posterior 2d-density for the locations of UDGs using all the non-empty samples of  $\mathbf{X}_c$ . We then compute the highest posterior density (HPD) region with some user-defined probability threshold  $\alpha$ , which we denote  $\text{HPD}(\alpha)$ , to predict UDG locations. Write

$$\text{HPD}(\alpha) = \bigcup_{k=1}^{K_\alpha} B_k, \text{ and } \forall 1 \leq k_1 \neq k_2 \leq K_\alpha, \text{dist}(B_{k_1}, B_{k_2}) > 0,$$

where

$$K_\alpha = \max_J \left\{ J : \bigcup_{j=1}^J B_j = \text{HPD}(\alpha), \forall 1 \leq j_1, j_2 \leq J, \text{dist}(B_{j_1}, B_{j_2}) > 0 \right\}.$$

$\text{dist}(A, B)$  is the distance between two sets  $A, B$  under the Euclidean metric.  $B_k$ 's are all the isolated sets that make up  $\text{HPD}(\alpha)$ , and each  $B_k$  represents the location of a potential UDG.

**4.2.2. Performance Metrics of UDG Detection.** We now introduce a novel set of performance metrics to assess the detection performance of a model by considering its *accuracy* and *precision*. Suppose a model produces  $\alpha$ -level HPD region  $\text{HPD}(\alpha)$  based on a set of GC data that contains  $n$  number of UDGs. Define  $C_i, i = 1, \dots, n$  as

$$C_i = \{s \in \mathbb{R}^2 : d(s, u_i) \leq R_{\text{eff}}^i\},$$

where  $d$  is the Euclidean metric,  $u_i$  is the reported location of the  $i$ -th known UDG, and  $R_{\text{eff}}^i$  is the effective radius<sup>3</sup> of the GC system of the  $i$ th-UDG.

For the accuracy measure of an algorithm, it contains the true-positive (TP) metric and the false-positive (FP) metric. We define the  $\alpha$ -level TP metric for an algorithm to be:

$$\text{TP}(\alpha) = \frac{1}{n} \sum_{i=1}^n |\mathbf{1}\{\text{HPD}(\alpha) \cap C_i \neq \emptyset\} - 1|.$$

This metric checks if  $\text{HPD}(\alpha)$  contains the locations of known UDGs. If locations of all UDGs in a field are contained in  $\text{HPD}(\alpha)$ , then  $\text{TP}(\alpha) = 0$  and the algorithm is accurate at  $\alpha$ -level. The TP metric is analogous to the bias of standard statistical estimators. We do

---

<sup>3</sup>Effective radius here is defined as the radius that contains half of the total number of GCs in a galaxy.

not check if  $\text{HPD}(\alpha)$  covers the exact reported locations  $u_i$ 's since (a) there is always some level of uncertainty on  $u_i$ 's; (b)  $\text{HPD}(\alpha)$  is obtained based on the information of GCs, and it may mismatch with the  $u_i$ 's that are determined by the light profiles of UDGs. Therefore, we check if  $\text{HPD}(\alpha)$  overlaps with circles  $C_i$ 's centered at the  $u_i$ 's. We set the radius of  $C_i$  to be the effective radius as this radius is not too big to cause false positive detection to become true positive detection but also not too small for the previously mentioned issues of (a) and (b) to occur. It is safe to assume  $\forall i, j \leq n, C_i \cap C_j = \emptyset$  since it would otherwise imply two UDGs are merging, which has never been observed. Although discovering merging UDGs are interesting, we do not consider it here.

We define the  $\alpha$ -level FP metric of an algorithm as

$$\text{FP}(\alpha) = \text{card}(\{B_k : B_k \cap (\cup_{i=1}^n C_i) = \emptyset\}).$$

The FP metric counts how many predicted UDGs by  $\text{HPD}(\alpha)$  are incorrect predictions. If  $\text{FP}(\alpha) = 0$ , then the algorithm produces no false positive detection at  $\alpha$ -level.

Aside from being accurate, we also require an algorithm to be precise so that we are certain about the predicted locations of UDGs. We thus consider the  $\alpha$ -level precision metric as:

$$\text{Prec}(\alpha) = \mu(\text{HPD}(\alpha)) / \mu(\cup_{i=1}^n C_i),$$

where  $\mu$  is the Lebesgue measure on  $\mathbb{R}^2$ . The precision metric checks how big  $\text{HPD}(\alpha)$  is and a precise algorithm should have small  $\text{Prec}(\alpha)$ . The ideal algorithm is to produce prediction of a point location of an UDG, which corresponds to  $\text{Prec}(\alpha) = 0$ , but this is impossible in reality. Note that the precision metric introduced here is normalized by the area of  $\cup_{i=1}^n C_i$  so that cross-comparison of precision between different data sets (if needed) is sensible.

**5. Data Analysis.** In this section, we apply the procedure of Section 4 to fit the models presented in Section 3 to a selected set of data described in Section 2. We select 12 of the 20 pointings in the data set. The selection details are deferred to later sections. We do not consider detecting GC-poor ( $N_{\text{GC}} \leq 2$ ) UDGs since the signals of these UDGs are too weak for any algorithm to detect, and an UDG with two GCs is indistinguishable from spurious clusters arising from pure randomness. Our analysis concludes the following: (i) our models correctly identify the existence of GC-rich UDGs; (ii) our models report a new potential UDG containing 3 GCs that is previously overlooked by the LGCP method in Li et al. (2022); (iii) Model 2 can indeed perform significantly better than Model 1, especially when UDGs reside in a noisy environment.

We run our MCMC algorithm with 100k iterations under Model 1 and Model 2 where the first 10k iterations are discarded as burn-in. To assess MCMC convergence of the two models, we compute an improved version of the Gelman-Rubin statistics ( $\hat{R}$ ; Gelman and Rubin, 1992) by Vats and Knudson (2021) for  $p_{i0}^1$  and  $p_{i0}^2$  mentioned in Section 3. We utilize Vats and Knudson's  $\hat{R}$  here since it can be computed using only one Markov chain, thus drastically reducing the computational cost of requiring multiple chains to conduct convergence diagnostics.  $p_{i0}^1$  and  $p_{i0}^2$  here are the full conditional probability that the  $i$ -th GC does not come from an UDG under Model 1 and Model 2 respectively. Due to the label-switching problem of RJMCMC-type algorithm, convergence diagnostic is typically hard.  $p_{i0}^1$  and  $p_{i0}^2$  are useful here for assessing MCMC convergence since they contain all model parameters whilst are also not subject to the label-switching problem. The computed  $\hat{R}$  for the membership probabilities of all GCs within the pointings considered are  $< 1.01$  under both Model 1 and Model 2, indicating sufficient convergence.

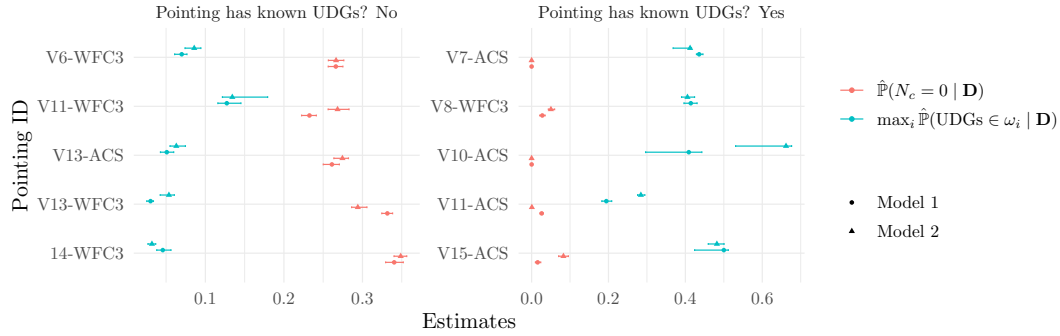


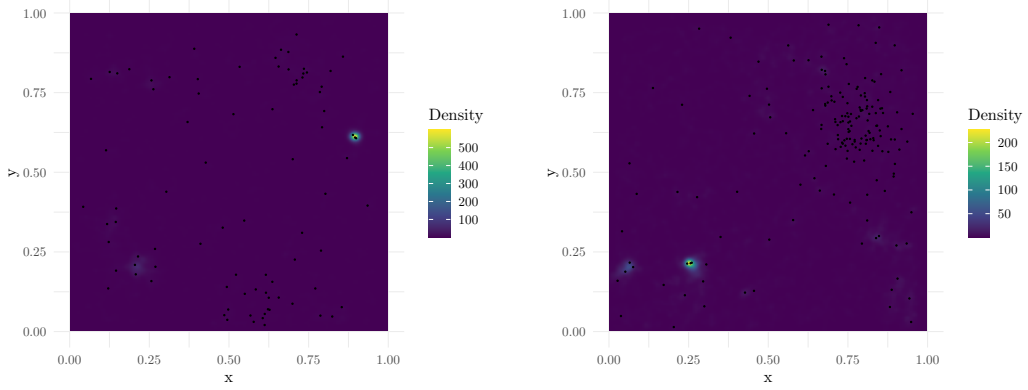
Fig 2: Posterior probabilities that a pointing does not contain an UDG and posterior probabilities that the pointing contains an UDG at a certain location for 10 selected pointings. Red indicates the probability of no UDGs from our models; blue indicates the probability that there is an UDG somewhere from our models. Points and triangles are the estimates under Model 1 and Model 2 respectively; error bars are the 95% block bootstrap confidence intervals for the estimates. Results here clearly indicate that both Model 1 and Model 2 correctly identify the existence of UDGs in all pointings.

5.1. *Whether a Pointing Contains an UDG.* Here we present the results from our models fitted to ten selected pointings. Five pointings do not contain known GC-rich UDGs while the other five do. There are other pointings without GC-rich UDGs, but these are not considered as they have too few number of GCs ( $\leq 20$ ) and the existence of GC-rich UDGs is so obvious that there is no need for any statistical machinery. The selection of pointings with known GC-rich UDGs are explained later while we compare the performance between Model 1 and Model 2 in Section 5.3.

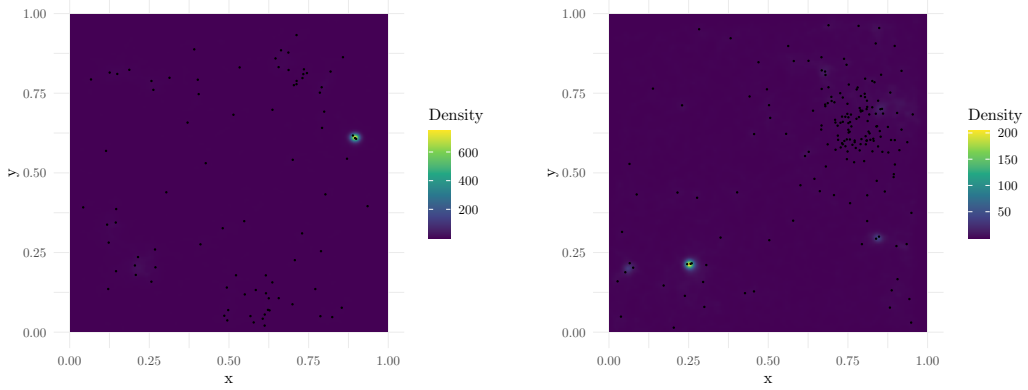
Figure 2 shows the results by fitting Model 1 and Model 2 to the aforementioned pointings and applying the procedures described in Section 4.2.1. The uncertainty of the posterior estimates are obtained using a block bootstrap conducted on the MCMC samples with the block size being 125. Figure 2 clearly shows that for pointings without known GC-rich UDGs, our models correctly identifies them as having no UDGs while for pointings that do contain known GC-rich UDGs, our models also made the correct identification. LGCP, on the other hand, simply does not have the capability to provide us with any quantitative insight on whether there are UDGs in a pointing at all.

5.2. *A Potential Dark Galaxy.* Our models also discovered a potential new dark galaxy overlooked by Li et al. using LGCP. This target resides in both the pointings V12-ACS and V14-ACS. Figure 3 shows the detection results comparison between our models and LGCP fitted to both pointings. From the figure, posterior mean of  $\exp(\mathcal{U}(s))$  from LGCP seems like pure random noise for both pointings. On the other hand, Figure 3(a), (b), (c), and (d) show that our models picked up a cluster of GCs with extremely strong signal located at the mid-right region of V12-ACS and at the lower-left region of V14-ACS. This cluster contains three tightly clumped GCs with no detectable diffuse light. A rough estimate<sup>4</sup> of the probability that this cluster is a result of pure random fluctuation from a Poisson process is  $\sim 0.0036$ . We dub this object Candidate Dark Galaxy-2 (CDG-2) following the discovery of another potential dark galaxy — CDG-1 by Li et al. (2022).

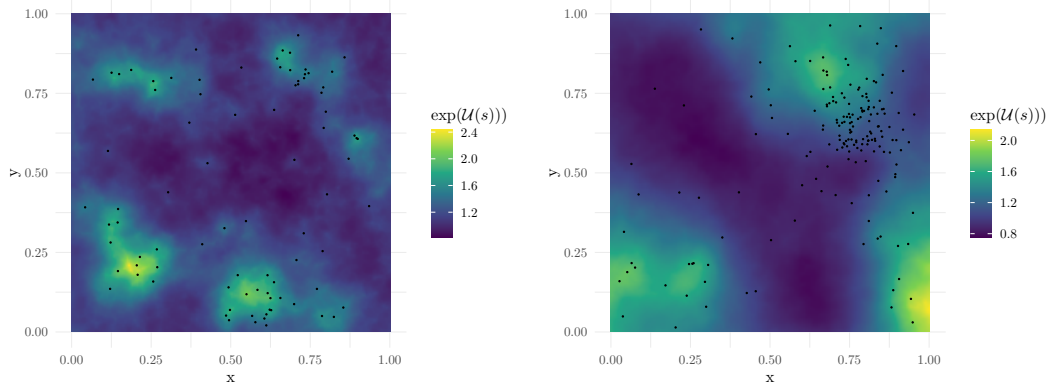
<sup>4</sup>See supplementary materials.



(a) Posterior density from Model 1 for V12-ACS (b) Posterior density from Model 1 for V14-ACS



(c) Posterior density from Model 2 for V12-ACS (d) Posterior density from Model 2 for V14-ACS



(e)  $\mathbb{E}(\exp(\mathcal{U}(s)) \mid \mathbf{X})$  from LGCP for V12-ACS (f)  $\mathbb{E}(\exp(\mathcal{U}(s)) \mid \mathbf{X})$  from LGCP for V14-ACS

Fig 3: Posterior detection results for CDG-2 using (a) Model 1 in V12-ACS; (b) Model 1 in V14-ACS; (c) Model 2 in V12-ACS; (d) Model 2 in V14-ACS; (e) LGCP in V12-ACS and (f) LGCP in V14-ACS. Black points are the locations of GCs in the pointing. The highest density region in the right of (a) and bottom-left of (b) is CDG-2. We see that LGCP fails to detect it in both V12 and V14-ACS.

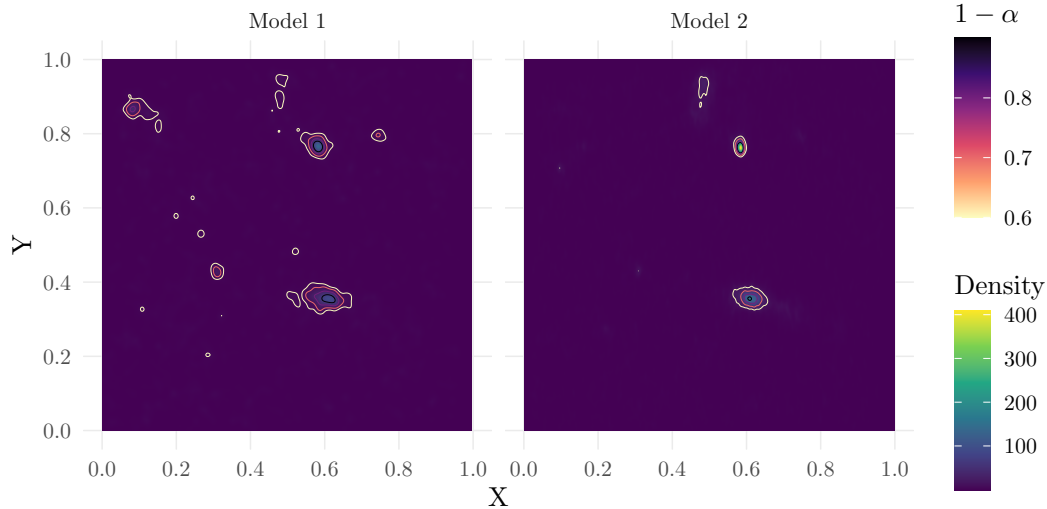
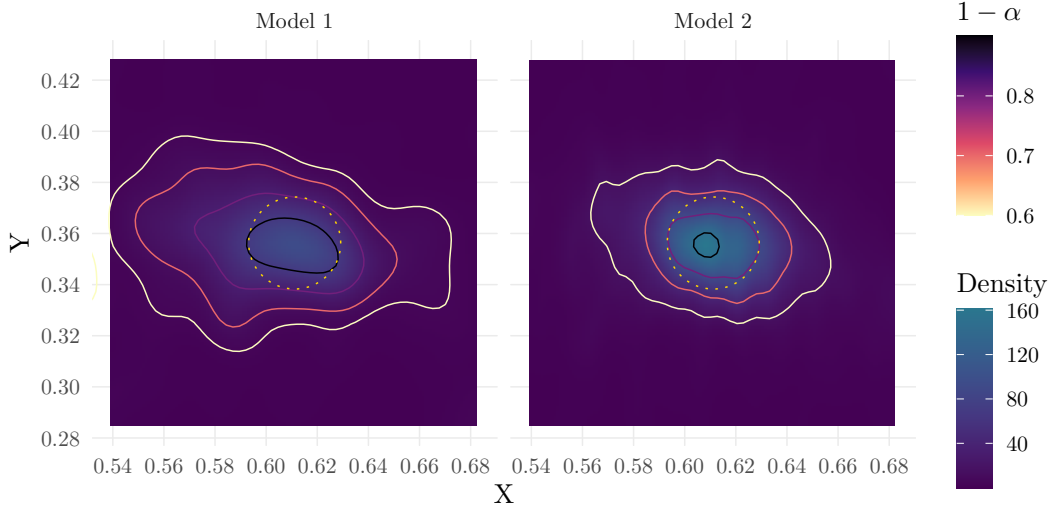


Fig 4: Posterior density of locations of UDGs for the field V11-ACS under Model 1 and Model 2. Contour lines show the HPD regions with probability levels  $\alpha = \{0.1, 0.2, 0.3, 0.4\}$ . Both models correctly detect the two UDGs in this field as indicated by the two highest density points in the figures. However, Model 2 clearly produces much fewer false positive detections.

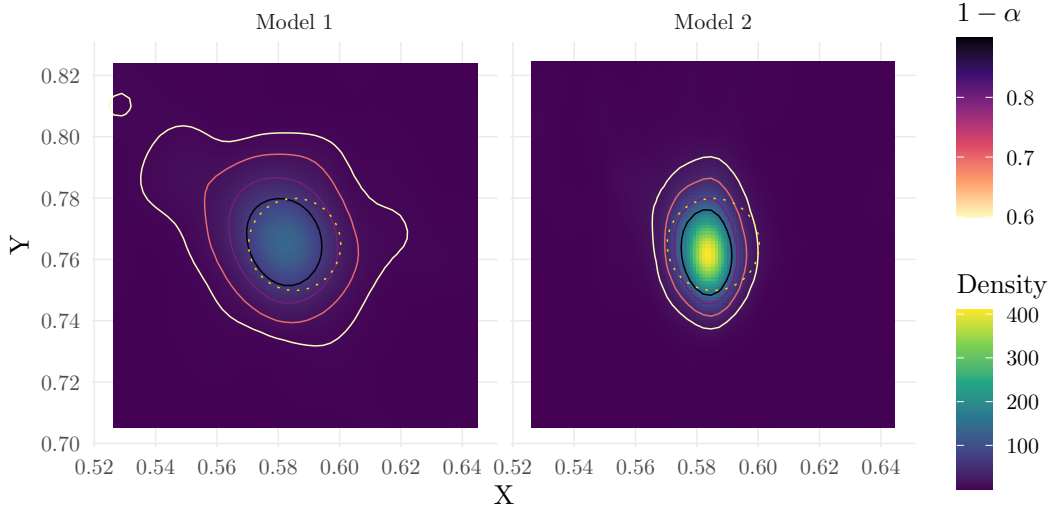
Note that the posterior density increased at CDG-2 for V12-ACS but decreased for V14-ACS under Model 2. This is due to the data inconsistency bound to happen occasionally in astronomical context rather than an issue of our models. Essentially, the colour data of GCs that overlap in the two pointings mismatch where one GC in CDG-2 has a colour of 1.455 in V12-ACS but 1.092 in V14-ACS for example. This mismatch in the colour effectively causes the colour variations of GCs in CDG-2 to be much larger in V14-ACS than in V12-ACS which leads to the opposite effect on signal strength of CDG-2 when GC colour information is included. Nonetheless, CDG-2 is still detected in both pointings and under both models.

On the other hand, LGCP fails at detecting CDG-2 in both pointings and this is likely due to the Gaussian random field structure. LGCP simply ignores weaker clustering signals such as CDG-2 as LGCP takes it as an inevitable fluctuation caused by the underlying Gaussian random field. Our models, on the other hand, do not encounter such an issue as it is always searching for clumps of points, even if their signals are relatively weak.

*5.3. Improving Detection Performance in Noisy Environments with Model 2.* To see whether Model 2 can improve detection performance in noisy environments, we consider pointings that contain more than one known GC-rich UDGs or pointings with known bright, normal galaxies. The UDGs in these pointings are more likely to be affected by noise or signals from other UDGs. Our selection resulted in five pointings. Other pointings with known UDGs are too "clean" for Model 2 to be useful at all. In fact, if a pointing is too "clean", it is not necessary to invoke any complex models. Figure 4 shows the posterior 2d-density of the potential locations of UDGs in the pointing V11-ACS, as well as the HPD regions computed with probability levels  $\alpha = \{0.1, 0.2, 0.3, 0.4\}$  under Model 1 and Model 2. The densities are constructed from a thinned sample using every five iteration of the MCMC sample for ease of computation. Figure 5 is a zoom-in version of Figure 4 focused on the locations of the two known UDGs in V11-ACS. To save space, we only present the figure for V11-ACS for demonstrative purposes since V11-ACS is the noisiest pointing of all.



(a) WUDG-88



(b) WUDG-89

Fig 5: Enlarged posterior density plots and the HPD regions based on Figure 4 for (a) WUDG-88 and (b) WUDG-89 in the field V11-ACS. Golden dotted circles show the locations of the two UDGs with radii being their respective effective radii. Model 2 clearly produces detections that are much more precise than Model 1.

In Figure 5, the golden dotted circles indicate the two known UDGs — WUDG-88 and WUDG-89 — in V11-ACS. From the two figures, it is clear that the estimated posterior densities at the locations of these two UDGs are much higher under Model 2 compared to Model 1. Based on Figure 4, we can see that when the probability levels  $\alpha$  are high, i.e., when the probability density cutoffs are low, Model 1 produces HPD regions that contain a lot of false positive detection regions while Model 2 produces HPD regions that have significantly fewer false positive regions. In terms of the true positive measure, Model 1 and Model 2 have the same performance across all levels of  $\alpha$  as they both manage to provide the correct locations of the two UDGs. However, Figure 5 shows that Model 2 is much more precise than

TABLE 1

Relative percentage increase in the precision measures from Model 1 to Model 2 for the five pointings considered. Estimates are given for each pointing for each value of  $\alpha$  considered. Brackets under the estimates are the 95% block bootstrap CIs of the estimates from the MCMC samples. A value greater than 0 means Model 2 is better. Teal coloured estimates represent Model 2 being significantly better than Model 1 at 5% level while purple coloured ones represent the opposite. Black estimates represent Model 1 and Model 2 are not significantly different. The pointings are ordered based on how noisy (total number of GCs  $N_{GC}$ ) they are. It is clear that the magnitude of improvement in precision increases with the noise level for four of the pointings.

Pointing	Prec <sub>1</sub> ( $\alpha$ )/Prec <sub>2</sub> ( $\alpha$ ) - 1 ( $\times 100\%$ )				$N_{GC}$
	$\alpha = 0.1$	$\alpha = 0.2$	$\alpha = 0.3$	$\alpha = 0.4$	
V7-ACS	2.44 (-5.86, 19.96)	9.79 (-0.27, 16.08)	8.22 (0.85, 13.07)	6.32 (1.24, 13.52)	61
V15-ACS	12.18 (1.26, 28.09)	16.06 (5.19, 23.84)	19.03 (3.34, 31.13)	16.18 (3.29, 35.35)	65
V10-ACS	12.34 (12.77, 43.79)	16.95 (9.3, 39.68)	22.32 (5.74, 41.99)	33.24 (0.68, 57.39)	109
V8-WFC3	-23.16 (-26.74, -6.74)	-19.98 (-26.76, -9.6)	-18.06 (-21.81, -2.9)	-16.0 (-39.53, 13.76)	164
V11-ACS	164.9 (129.1, 199.6)	156.0 (122.06, 184.63)	180.2 (136.5, 221.2)	204.5 (148.05, 248.8)	262

Model 1 as the sizes of the HPD regions from Model 2 are at least twice as small as Model 1 for all values of  $\alpha$  considered.

In terms of TP measures, all UDGs within the five pointings are correctly detected by both models across all probability level  $\alpha$  except for V7-ACS when  $\alpha = 0.1$ . V7-ACS contains two UDGs with one having a weaker signal than the other, and Model 1 fails to detect the weaker one when  $\alpha = 0.1$  with 80% confidence. This is likely because the inclusion of GC colour information boosts the signal strength of the weaker UDG. For FP measures, both models have the same performance except for V11-ACS as demonstrated previously where Model 2 produces much fewer false positive detections than Model 1.

The precision measure comparison for the five pointings considered are given in Table 1 where we provide the relative percentage change in the precision measures from Model 1 to Model 2. For the confidence intervals of the relative change, we carry out a block resampling bootstrap using the thinned MCMC sample with the block size being 25.

From Table 1, Model 2 is significantly more precise than Model 1 for four out of the five pointings across nearly all probability level  $\alpha$ . This shows that Model 2 is indeed capable of improving the certainty of UDG detection. We will discuss the worsening performance from V8-WFC3 separately in the latter part of the section.

Interestingly, Model 2 seems to produce a rather small or insignificant amount of improvement over Model 1 for the pointing V7-ACS compared to other pointings. We believe this is because V7-ACS is the most noiseless pointing among the five that we considered, while the clustering signals of GCs in the UDGs of V7-ACS are exceptionally strong. In such a scenario, the additional information of GC colour information would only bring forth a marginal amount of improvement. However, Model 2 is not designed with the intention to detect UDGs in a noiseless or nearly noiseless situations, but to improve the detection for noisy pointings. This is highly desired since the main task of UDG detection will be conducted within the noisy environment regimes. The results presented in Table 1 show that Model 2 indeed does what we intend it to do: for the four pointings where Model 2 is better, the magnitude of the improvement produced by Model 2 increases as the number of total GCs in a pointing increases, i.e., increasing noise level.

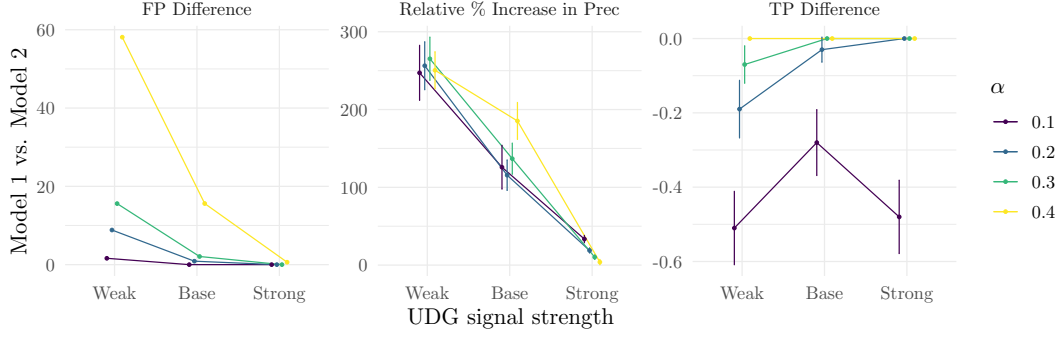


Fig 6: Estimated mean performance metrics comparison between Model 1 and Model 2 obtained from the simulations. For FP and precision metrics, above zero means Model 2 is better while below zero means Model 1 is better for TP metric. Error bars are the 95% CIs of the mean estimates.

Due to computational constraint, we conduct three sets of simulations using the field V11-ACS to verify that Model 2 indeed produces more improvement when pointings get noisier. For the base set of simulation, we set the point pattern of GCs to be the same as in V11-ACS, while replacing the colour of the GCs in the known UDGs by simulated ones. The simulated colours are generated from a normal distribution with mean and standard deviation estimated using the colour of GCs from the known UDGs. The colours of other non-UDG GCs remain the same as in the real data since this keeps our simulations as close to reality as possible. Model 2 is then fitted to the simulated data and performance comparison is computed against results from Model 1. We do this for 100 times. For the rest of the two simulation sets, we simulate UDGs with weaker and stronger GC clustering signals while keeping the non-UDG GC point pattern the same as in the real data. We simulate UDGs with different signal strengths instead of different noise levels since it is much easier to generate simulated data that is closer to reality for the former. Moreover, the effect of noise is opposite to the effect of signal strength of an UDG since increasing the UDG signal strength are equivalent to decreasing noise level. For the simulation set with weaker UDG signals, we remove one GC from each of the two known UDGs. For the other simulation set, we replace them with simulated UDGs but with two more GCs in each UDG to emulate stronger signal strengths. The colour simulation schemes for the latter two simulation sets are the same as for the base simulation set. Each set also contains 100 simulations. Note that the GC point pattern remains the same within each simulation set as we are interested in how including colour affects the performance, thus the variation caused by simulating GC point patterns need to be excluded.

If Model 2 indeed performs better in noisier pointings, or equivalently when the signal strength of an UDG is weaker, then we would expect the average improvement in performance should increase as the signal strengths of UDGs decrease, especially for the precision measure.

Figure 6 shows the estimated mean comparison between Model 1 and Model 2 for the three performance metrics from simulations. We can clearly see that for the FP and precision metrics, the average amount of improvement achieved by Model 2, i.e., by including GC colour, increases significantly as the signal strengths of UDGs decreases. This results confirm our previous observation found in Table 1, and we are provided with sufficient evidence that Model 2 can be much more effective at detecting UDGs in noisier environments. Interestingly, the results of the TP metric indicate that Model 2 is worse than Model 1 sometimes. This is somewhat inevitable as there are two UDGs with different signal strengths in the simulations: adding the GC colour information may sometimes lead to unbalanced increase in

signal strengths for the two UDGs that one of the UDGs is missed, especially when the probability threshold  $\alpha$  is low. In fact, arbitrarily low  $\alpha$  will inevitably only be able to detect one UDG at best regardless of which of the two models is used. Hence, it is preferable to consider higher values of  $\alpha$  in case we miss some of the UDGs. Thus, Model 2 proves to be even more useful since if we increase  $\alpha$ , the number of false positive detections will inevitably increase. Model 2 then can control the false positive rates at a significantly lower level than Model 1 as shown in Figure 6.

Lastly, for V8-WFC3, Model 2 is being outperformed by Model 1 in terms of the precision measure shown in Table 1. This is because the UDG in the pointing has five GCs where the GC colour variations for two of these GCs are much larger than the rest. This led to the UDG having a weaker detection signal under Model 2. As mentioned, the assumption where GC colour variations being smaller than that of GCs in other environments is not always guaranteed. There will always be UDGs having large GC colour variations, but these UDGs are within the minority and Model 2 would be highly useful in majority of the cases.

**6. Conclusion & Future Works.** In this paper, we introduced a set of novel point process models under the framework of PCP to detect ultra-diffuse galaxies through their globular clusters. We fitted our model to a set of real data using an improved spatial birth-death-move MCMC algorithm. We demonstrated that our models perfectly resolve the issues of LGCP method where LGCP does not have the ability to identify the non-existence of UDGs and can potentially miss UDGs with weak signals. Moreover, the novel marked point process model with GC colour information incorporated proves to have the ability to significantly improve the detection signals of UDGs in noisy environments. In the future, there are several directions of research: (a) we intend to apply our model to massive all-sky survey to search for UDGs in the nearby Universe ( $d \sim 2 - 5$  Mpc), such an endeavor could potentially reveal new UDGs that have eluded astronomers previously due to the limitations of the current method of finding UDGs through their associated diffuse stellar light; (b) we also hope to further improve the inference algorithm by increasing the computational speed: the main computational bottleneck of our algorithm is the integration of the intensity function in our model. The integration scheme currently used is the simple grid-based method. Such a method is quite wasteful as a very high number of grids is required to obtain accurate result but the majority of the grids do not have significant contribution to the final integral. An adaptive scheme that can carry out fast and accurate integration can speed up the algorithm significantly.

## REFERENCES

- ABRAHAM, R. G. and VAN DOKKUM, P. G. (2014). Ultra-Low Surface Brightness Imaging with the Dragonfly Telephoto Array. *PASP* **126** 55. <https://doi.org/10.1086/674875>
- AMORISCO, N. C., MONACHESI, A., AGNELLO, A. and WHITE, S. D. M. (2018). The globular cluster systems of 54 Coma ultra-diffuse galaxies: statistical constraints from HST data. *MNRAS* **475** 4235-4251. <https://doi.org/10.1093/mnras/sty116>
- BERTIN, E. and ARNOUTS, S. (1996). SExtractor: Software for source extraction. *A&AS* **117** 393-404. <https://doi.org/10.1051/AAS:1996164>
- BINGGELI, B., SANDAGE, A., TARENGHI, M., BINGGELI, B., SANDAGE, A. and TARENGHI, M. (1984). Studies of the Virgo Cluster. I. Photometry of 109 galaxies near the cluster center to serve as standards. *AJ* **89** 64-82. <https://doi.org/10.1086/113484>
- BOLIN, D. and LINDGREN, F. (2015). Excursion and contour uncertainty regions for latent Gaussian models. *J. R. Stat. Soc. Ser. B Methodol* **77** 85-106. <https://doi.org/10.1111/rssb.12055>
- BOLIN, D. and LINDGREN, F. (2018). Calculating Probabilistic Excursion Sets and Related Quantities Using excursions. *J. Stat. Softw.* **86** 1-20. <https://doi.org/10.18637/JSS.V086.I05>
- BURKERT, A. (2017). The Geometry and Origin of Ultra-diffuse Ghost Galaxies. *ApJ* **838** 93. <https://doi.org/10.3847/1538-4357/AA671C>

- BURKERT, A. (2020). Fuzzy Dark Matter and Dark Matter Halo Cores. *ApJ* **904** 161. <https://doi.org/10.3847/1538-4357/abb242>
- CANNON, J. M., MARTINKUS, C. P., LEISMAN, L., HAYNES, M. P., ADAMS, E. A. K., GIOVANELLI, R., HALLENBECK, G., JANOWIECKI, S., JONES, M., JÓZSA, G. I. G., KOOPMANN, R. A., NICHOLS, N., PAPASTERGIS, E., RHODE, K. L., SALZER, J. J. and TROISCHT, P. (2015). The ALFALFA "Almost Dark" Campaign: Pilot VLA HI Observations of Five High Mass-to-Light Ratio Systems. *AJ* **149** 72. <https://doi.org/10.1088/0004-6256/149/2/72>
- CASTELLOE, J. (1998). Issues in reversible jump Markov chain Monte Carlo and composite EM analysis, applied to spatial Poisson cluster processes, PhD thesis, University of Iowa.
- DANIELI, S., VAN DOKKUM, P., TRUJILLO-GOMEZ, S., KRUIJSSEN, J. M. D., ROMANOWSKY, A. J., CARLSTEN, S., SHEN, Z., LI, J., ABRAHAM, R., BRODIE, J., CONROY, C., GANNON, J. S. and GRECO, J. (2021). NGC5846-UDG1: A galaxy formed mostly by star formation in massive, extremely dense clumps of gas.
- DIGGLE, P. J., MORAGA, P., ROWLINGSON, B. and TAYLOR, B. M. (2013). Spatial and Spatio-Temporal Log-Gaussian Cox Processes: Extending the Geostatistical Paradigm. *Statistical Science* **28** 542–563.
- FORBES, D. A. (2017). How large are the globular cluster systems of early-type galaxies and do they scale with galaxy halo properties? *MNRAS* **472** L104–L108. <https://doi.org/10.1093/MNRASL/SLX148>
- GBHARDT, K. and KISSLER-PATIG, M. (1999). Globular Cluster Systems. I. VI Color Distributions. *AJ* **118** 1526–1541. <https://doi.org/10.1086/301059>
- GELMAN, A. and RUBIN, D. B. (1992). Inference from Iterative Simulation Using Multiple Sequences. *Stat Sci* **7** 457–472. <https://doi.org/10.1214/ss/1177011136>
- GENG, J., SHI, W. and HU, G. (2021). Bayesian nonparametric nonhomogeneous Poisson process with applications to USGS earthquake data. *Spatial Statistics* **41** 100495. <https://doi.org/10.1016/J.SPASTA.2021.100495>
- GREEN, P. J. (1995). Reversible jump Markov chain Monte Carlo computation and Bayesian model determination. *Biometrika* **82** 711–732. <https://doi.org/10.1093/biomet/82.4.711>
- GUDEHUS, D. (1995). The Virgocentric velocity from bright cluster galaxies. *A&A* **302** 21.
- HARRIS, E. W. (1991). Globular cluster systems in galaxies beyond the Local Group. *ARA&A* **29** 543–579. <https://doi.org/10.1146/ANNUREV.AA.29.090191.002551>
- HARRIS, W. E., HARRIS, G. L. H. and ALESSI, M. (2013). A Catalog of Globular Cluster Systems: What Determines the Size of a Galaxy's Globular Cluster Population? *ApJ* **772** 82. <https://doi.org/10.1088/0004-637x/772/2/82>
- HARRIS, W. E., BROWN, R. A., DURRELL, P. R., ROMANOWSKY, A. J., BLAKESLEE, J., BRODIE, J., JANSSENS, S., LISKER, T., OKAMOTO, S. and WITTMANN, C. (2020). The PIPER Survey. I. An Initial Look at the Intergalactic Globular Cluster Population in the Perseus Cluster. *ApJ* **890** 105. <https://doi.org/10.3847/1538-4357/ab6992>
- HUDSON, M. J., LUCEY, J. R., SMITH, R. J., STEEL, J., HUDSON, M. J., LUCEY, J. R., SMITH, R. J. and STEEL, J. (1997). Galaxy clusters in the Perseus-Pisces region - II. The peculiar velocity field. *MNRAS* **291** 488–504. <https://doi.org/10.1093/MNRAS/291.3.488>
- HUI, L., OSTRIKER, J. P., TREMAINE, S. and WITTEN, E. (2017). Ultralight scalars as cosmological dark matter. *Phys. Rev. D* **95** 043541. <https://doi.org/10.1103/PHYSREVD.95.043541/FIGURES/3/MEDIUM>
- JANOWIECKI, S., LEISMAN, L., JÓZSA, G., SALZER, J. J., HAYNES, M. P., GIOVANELLI, R., RHODE, K. L., CANNON, J. M., ADAMS, E. A. K. and JANESH, W. F. (2015). (Almost) Dark HI Sources in the ALFALFA Survey: The Intriguing Case of HI1232+20. *ApJ* **801** 96. <https://doi.org/10.1088/0004-637x/801/2/96>
- JANSSENS, S. R., ABRAHAM, R., BRODIE, J., FORBES, D. A. and ROMANOWSKY, A. J. (2019). The Distribution of Ultra-Diffuse and Ultra-Compact Galaxies in the Frontier Fields. *ApJ* **887** 92. <https://doi.org/10.3847/1538-4357/ab536c>
- JASRA, A., HOLMES, C. C. and STEPHENS, D. A. (2005). Markov Chain Monte Carlo Methods and the Label Switching Problem in Bayesian Mixture Modeling. *Stat. Sci.* **20** 50–67.
- LI, D. D., EADIE, G. M., ABRAHAM, R., BROWN, P. E., HARRIS, W. E., JANSSENS, S. R., ROMANOWSKY, A. J., VAN DOKKUM, P. and DANIELI, S. (2022). Light from the Darkness: Detecting Ultra-diffuse Galaxies in the Perseus Cluster through Over-densities of Globular Clusters with a Log-Gaussian Cox Process. *ApJ* **935** 3. <https://doi.org/10.3847/1538-4357/AC7B22>
- LIM, S., PENG, E. W., CÔTÉ, P., SALES, L. V., DEN BROK, M., BLAKESLEE, J. P. and GUHATHAKURTA, P. (2018). The Globular Cluster Systems of Ultra-diffuse Galaxies in the Coma Cluster. *ApJ* **862** 82. <https://doi.org/10.3847/1538-4357/AACB81>
- LIM, S., CÔTÉ, P., PENG, E. W., FERRARESE, L., ROEDIGER, J. C., DURRELL, P. R., MIHOS, J. C., WANG, K., GWYN, S. D. J., CUILLANDRE, J.-C., LIU, C., SÁNCHEZ-JANSSEN, R., TOLOBA, E., SALES, L. V., GUHATHAKURTA, P., LANÇON, A. and PUZIA, T. H. (2020). The Next Generation Virgo Cluster Survey (NGVS). XXX. Ultra-diffuse Galaxies and Their Globular Cluster Systems. *ApJ* **899** 69. <https://doi.org/10.3847/1538-4357/ABA433>

- LOTZ, J. M., MILLER, B. W. and FERGUSON, H. C. (2004). The Colors of Dwarf Elliptical Galaxy Globular Cluster Systems, Nuclei, and Stellar Halos. *ApJ* **613** 262–278. <https://doi.org/10.1086/422871/FULLTEXT/>
- MARTÍNEZ-DELGADO, D., LÄSKER, R., SHARINA, M., TOLOBA, E., FLIRI, J., BEATON, R., VALLS-GABAUD, D., KARACHENTSEV, I. D., CHONIS, T. S., GREBEL, E. K., FORBES, D. A., ROMANOWSKY, A. J., GALLEGGO-LABORDA, J., TEUWEN, K., GÓMEZ-FLECHOSO, M. A., WANG, J., GUHATHAKURTA, P., KAISIN, S. and HO, N. (2016). Discovery of an Ultra-Diffuse Galaxy in the Pisces-Perseus Supercluster. *AJ* **151** 96. <https://doi.org/10.3847/0004-6256/151/4/96>
- MØLLER, J., SYVERSVEEN, A. R. and WAAGEPETERSEN, R. P. (1998). Log Gaussian Cox processes. *Scand. J. Stat.* **25** 451–482. <https://doi.org/10.1111/1467-9469.00115>
- MØLLER, J. (2003). Shot Noise Cox Processes. *Adv Appl Probab* **35** 614–640.
- MØLLER, J. and TOFTAKER, H. (2014). Geometric Anisotropic Spatial Point Pattern Analysis and Cox Processes. *Scand. J. Stat.* **41** 414–435. <https://doi.org/10.1111/SJOS.12041>
- MØLLER, J. and TORRISI, G. L. (2005). Generalised Shot Noise Cox Processes. *Adv Appl Probab* **37** 48–74.
- OOSTERLOO, T. A. , HEALD, G. H. and DE BLOK, W. J. G. (2013). Is GBT5+5439 a dark galaxy? *A&A* **555** L7. <https://doi.org/10.1051/0004-6361/201321965>
- PENG, E. W. and LIM, S. (2016). A Rich Globular Cluster System in Dragonfly-17: Are Ultra-Diffuse Galaxies Pure Stellar Halos?\*. *ApJL* **822** L31. <https://doi.org/10.3847/2041-8205/822/2/L31>
- PROLE, D. J., VAN DER BURG, R. F. J., HILKER, M. and DAVIES, J. I. (2019). Observational properties of ultra-diffuse galaxies in low-density environments: field UDGs are predominantly blue and star forming. *MNRAS* **488** 2143–2157. <https://doi.org/10.1093/MNRAS/STZ1843>
- ROBERTS, G. O. and ROSENTHAL, J. S. (2009). Examples of Adaptive MCMC. *J. Comput. Graph. Stat.* **18** 349–367. <https://doi.org/10.1198/jcgs.2009.06134>
- SÉRSIC, J. L. (1963). Influence of the atmospheric and instrumental dispersion on the brightness distribution in a galaxy. *BAAA* **6** 41–43.
- SHEN, S., MO, H. J., WHITE, S. D. M., BLANTON, M. R., KAUFFMANN, G., VOGES, W., BRINKMANN, J. and CSABAI, I. (2003). The size distribution of galaxies in the Sloan Digital Sky Survey. *MNRAS* **343** 978–994.
- VAN DOKKUM, P. G., ABRAHAM, R., MERRITT, A., ZHANG, J., GEHA, M. and CONROY, C. (2015). Forty-Seven Milky Way-Sized, Extremely Diffuse Galaxies in the Coma Cluster. *ApJL* **798** L45. <https://doi.org/10.1088/2041-8205/798/2/L45>
- VAN DOKKUM, P., ABRAHAM, R., BRODIE, J., CONROY, C., DANIELI, S., MERRITT, A., MOWLA, L., ROMANOWSKY, A. and ZHANG, J. (2016). A high stellar velocity dispersion and  $\sim 100$  globular clusters for the ultra-diffuse galaxy Dragonfly 44. *ApJL* **828** L6. <https://doi.org/10.3847/2041-8205/828/1/L6>
- VAN DOKKUM, P., COHEN, Y., DANIELI, S., KRUIJSSEN, J. M. D., ROMANOWSKY, A. J., MERRITT, A., ABRAHAM, R., BRODIE, J., CONROY, C., LOKHORST, D., MOWLA, L., O’SULLIVAN, E. and ZHANG, J. (2018). An Enigmatic Population of Luminous Globular Clusters in a Galaxy Lacking Dark Matter. *ApJ* **856** L30. <https://doi.org/10.3847/2041-8213/aab60b>
- VAN DOKKUM, P., WASSERMAN, A., DANIELI, S., ABRAHAM, R., BRODIE, J., CONROY, C., FORBES, D. A., MARTIN, C., MATUSZEWSKI, M., ROMANOWSKY, A. J. and VILLAUME, A. (2019). Spatially Resolved Stellar Kinematics of the Ultra-diffuse Galaxy Dragonfly 44. I. Observations, Kinematics, and Cold Dark Matter Halo Fits. *ApJ* **880** 91. <https://doi.org/10.3847/1538-4357/ab2914>
- VATS, D. and KNUDSON, C. (2021). Revisiting the Gelman–Rubin Diagnostic. *Stat Sci* **36** 518 – 529. <https://doi.org/10.1214/20-STSS812>
- VENHOLA, A., PELETIER, R., LAURIKAINEN, E., SALO, H., LISKER, T., IODICE, E., CAPACCIOLI, M., KLEIJN, G. V., VALENTIJN, E., MIESKE, S., HILKER, M., WITTMANN, C., VAN DE VEN, G., GRADO, A., SPAVONE, M., CANTIELLO, M., NAPOLITANO, N., PAOLILLO, M. and FALCÓN-BARROSO, J. (2017). The Fornax Deep Survey with VST - III. Low surface brightness dwarfs and ultra diffuse galaxies in the center of the Fornax cluster. *A&A* **608** A142. <https://doi.org/10.1051/0004-6361/201730696>
- WAAGEPETERSEN, R. P. (2007). An Estimating Function Approach to Inference for Inhomogeneous Neyman-Scott Processes. *Biometrics* **63** 252–258.
- WANG, Q., PENG, E. W., BLAKESLEE, J. P., CÔTÉ, P., FERRARESE, L., JORDÁN, A., MEI, S. and WEST, M. J. (2013). The ACS Virgo Cluster Survey. XVII. The Spatial Alignment of Globular Cluster Systems with Early-Type Host Galaxies. *ApJ* **769** 145. <https://doi.org/10.1088/0004-637x/769/2/145>
- WANG, Y., DEGLERIS, A., WILLIAMS, A. H. and LINDERMAN, S. W. (2022). Spatiotemporal Clustering with Neyman-Scott Processes via Connections to Bayesian Nonparametric Mixture Models. <https://doi.org/10.48550/arxiv.2201.05044>
- WASSERMAN, A., VAN DOKKUM, P., ROMANOWSKY, A. J., BRODIE, J., DANIELI, S., FORBES, D. A., ABRAHAM, R., MARTIN, C., MATUSZEWSKI, M., VILLAUME, A., TAMANAS, J. and PROFUMO, S. (2019). Spatially Resolved Stellar Kinematics of the Ultra-diffuse Galaxy Dragonfly 44. II. Constraints on Fuzzy Dark Matter. *ApJ* **885** 155. <https://doi.org/10.3847/1538-4357/ab3eb9>

- WITTMANN, C., LISKER, T., TILAHUN, L. A., GREBEL, E. K., CONSELICE, C. J., PENNY, S., JANZ, J., GALLAGHER, J. S., KOTULLA, R. and MCCORMAC, J. (2017). A population of faint low surface brightness galaxies in the Perseus cluster core. *MNRAS* **470** 1512–1525. <https://doi.org/10.1093/mnras/stx1229>
- YAGI, M., KODA, J., KOMIYAMA, Y. and YAMANOI, H. (2016). Catalog of Ultra-Diffuse Galaxies in the Coma Clusters from Subaru Imaging Data\*. *ApJS* **225** 11. <https://doi.org/10.3847/0067-0049/225/1/11>